Demonstration of a tunable interface between Rydberg atoms and superconducting microwave circuits with differential polarizability nulling

L. L. Brown,[1] J. A. L. Grondin,[1,2,*] and S. D. Hogan[1]

[1]*Department of Physics and Astronomy, University College London, Gower Street, London WC1E 6BT, United Kingdom*

[2]*Université Rennes, CNRS, Institut FOTON–UMR 6082, 35000 Rennes, France*

(Received 10 April 2024; accepted 31 July 2024; published 19 August 2024)

Microwave-dressed Rydberg atoms in pairs of states that are optically accessible and engineered so that the frequency of the transition between them is tunable while exhibiting a low sensitivity to stray electric fields have been interfaced with a superconducting coplanar waveguide (CPW) microwave resonator. This was achieved with helium atoms in triplet Rydberg states with principal quantum numbers $n = 55$ and 56. The atoms were dressed with two strong microwave fields—a control field and a differential polarizability nulling field. The control field allowed the atoms to be coupled to the resonator using the two-color two-photon transition between the equal parity $1s55s\ ^3S_1 \equiv |55s\rangle$ and $1s56s\ ^3S_1 \equiv |56s\rangle$ Rydberg states, with one photon supplied by it and the other provided by the resonator. The nulling field was detuned from the field-free $1s55s\ ^3S_1 \rightarrow 1s55p\ ^3P_J \equiv |55p\rangle$ transition to admix $|55p\rangle$ character into the $|55s\rangle$ state and eliminate the differential static electric dipole polarizability of the $|55s\rangle$ and $|56s\rangle$ states. The experiments were performed with atoms located ∼300 μm above a $\lambda/4$ niobium nitride superconducting CPW resonator operated at temperatures between 3.59 and 3.73 K. The measured ac and dc Stark shifts of the Rydberg states at this atom-circuit interface in the presence of the dressing fields are in good quantitative agreement with the results of Floquet calculations. The differential polarizability nulling fields used in the experiments allowed the difference in the Stark shifts of the $|55s\rangle$ and $|56s\rangle$ states over the range of dc fields offset from the residual stray field by ±65 mV/cm to be reduced from $2\pi \times 2.1$ MHz to $2\pi \times 125$ kHz.

DOI: 10.1103/PhysRevA.110.022615

I. INTRODUCTION

Recently, significant progress has been made in interfacing gas-phase Rydberg atoms with solid-state superconducting microwave circuits for applications in hybrid quantum information processing. Experiments were performed with atoms in beams [1–3] and on superconducting atom chips [4]. In both cases, transitions between pairs of Rydberg states were coherently driven using the evanescent field in a single mode of a superconducting coplaner waveguide (CPW) microwave resonator. These resonators operate at angular frequencies of $\sim 2\pi \times 10$ GHz, which are compatible with transitions in Rydberg atoms and in superconducting qubits [5]. They also have small mode volumes $V \simeq 10^{-12}\,\mathrm{m}^3$, which lead to high microwave field amplitudes F_μ. For example, the typical amplitude of the field associated with a single photon in a CPW resonator of this kind is $F_\mu = \sqrt{\hbar\omega/2\epsilon_0 V} \simeq 10\,\mathrm{mV/cm}$ [6]. These strong fields, together with the large electric dipole moments for transitions between Rydberg states (e.g., $\mu_{\mathrm{elec}} \sim 2500 e a_0$ for the $1s55s\ ^3S_1 \rightarrow 1s55p\ ^3P_2$ transition in helium) or the quantized levels in superconducting qubits, provide opportunities to access the single-photon strong-coupling regime in this hybrid cavity QED setting and open a range of applications in quantum information processing [7].

Rydberg-atom–superconducting-circuit interfaces are of interest for the coherent transfer of quantum information between neutral "Rydberg"-atom qubits and superconducting qubits [8,9]. In this setting, the superconducting CPW resonator acts as a quantum bus. Proposals have been put forward to use these interfaces to implement quantum memories [8,10], for microwave-to-optical photon transduction through coherent multiwave mixing [11–13], and to enable long-range cavity-mediated interactions between neutral atoms [14–17]. They therefore also offer routes to networking spatially separated neutral-atom and superconducting quantum processors.

Access to the single-photon strong-coupling regime at a Rydberg-atom–superconducting-circuit interface requires effects of stray electric fields, caused by adsorbates and charge buildup on the cryogenically cooled superconducting chip surfaces, to be carefully managed [2,18,19]. To achieve this, pairs of Rydberg states must be selected with a low differential static electric dipole polarizability, i.e., similar Stark shifts in weak dc electric fields. The transitions between such states have low sensitivities to residual uncanceled stray electric fields and have enabled coherent atom-resonator coupling at distances of ∼300 μm from the surface of superconducting chips [3]. The coherence times in these experiments could be separated into a contribution from the dephasing of the atom–resonator-field interaction, which occurred on a timescale of

*Present address: KU Leuven, Instituut voor Kern- en Stralingsfysica, 3001 Leuven, Belgium.

~800 ns, and decoherence of the atomic superposition states generated upon the interaction of the atoms with the resonator field ($\gtrsim$2.5 μs). The former was attributed to the inhomogeneity of the microwave field across the distribution of atom positions above the resonator. The measurement of the latter was limited by the motion of the beam of atoms above the resonator. These coherence times will be extended in the future by working with colder atoms, however, to maximize the coupling strength between the atoms and the resonator field, it is necessary to minimize the atom-resonator distance. For example, in resonator geometries typically used in these experiments, vacuum Rabi frequencies of $2\pi \times (1-10)$ MHz are expected to be achievable at atom-resonator distances of 30–50 μm [20]. Performing experiments in this regime requires (1) the possibility to adjust, or tune, the frequency of the transition between the Rydberg states and (2) quantum-state engineering to minimize the sensitivity of the atoms to residual stray electric fields.

Here, we report a breakthrough in this area by demonstrating that a tunable interface between Rydberg atoms and superconducting circuits with significantly reduced sensitivity to stray electric fields can be realized by introducing two strong microwave-dressing fields in the volume above a superconducting CPW resonator. One of these fields acts as a strong control field to permit a two-photon transition between Rydberg states of equal parity to be driven as a two-color transition and the atoms to be coupled to the resonator field through the absorption of only one photon from it. This makes the interface widely tunable. The other dressing field is used to engineer the energy-level structure of the atoms to eliminate the differential static electric dipole polarizability of the Rydberg states. This approach to polarizability nulling of transitions between Rydberg states was initially suggested in the context of coherence-preserving Rydberg-atom trap architectures [21] and subsequently demonstrated in free-space experiments with rubidium [22,23], cesium [24,25], and helium [26].

In the following, the apparatus used in the experiments is described in Sec. II. In Sec. III, details of the microwave-dressing schemes implemented to tune and engineer the transitions between the Rydberg states, and the methods of calculation used to determine the optimal dressing-field parameters are presented. Experiments performed to demonstrate the tunable interface and the benefits of differential polarizability nulling are discussed in Secs. IV and V, respectively. Finally, in Sec. VI conclusions are drawn.

II. EXPERIMENT

A schematic diagram of the apparatus used in the experiments is shown in Fig. 1. This apparatus was similar to that described previously [1], but with adaptations to include an antenna to introduce microwave-dressing fields in the region above the superconducting chip.

Supersonic beams of helium were generated with mean longitudinal speeds of ~2000 m/s using a pulsed valve operated at a repetition rate of 25 Hz. A dc electric discharge was implemented at the exit of the valve to populate the metastable $1s2s\,^3S_1$ level [27]. After collimation at a 3-mm-diameter skimmer and the removal of charged particles

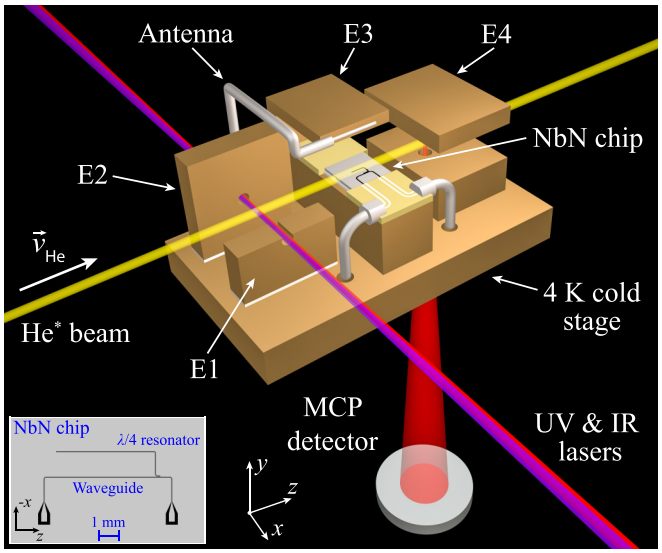

FIG. 1. Schematic diagram of the central cryogenic region of the experimental apparatus. For clarity, parts of electrode E1 and the split electrode E3 have been omitted. The MCP detector was located outside the cryogenic region of the apparatus and operated at room temperature. The geometry of the superconducting circuit on the NbN chip is shown schematically in the inset in the bottom left corner.

produced in the discharge using an electrostatic filter, the beams entered through apertures in two heat shields, operated at ~30 and ~4 K, and into the cryogenic region of the apparatus in Fig. 1. In this region, bunches of atoms were laser photoexcited to the $1s55s\,^3S_1 \equiv |55s\rangle$ Rydberg level between the electrodes labeled E1 and E2. This was achieved using the $1s2s\,^3S_1 \rightarrow 1s3p\,^3P_2 \rightarrow 1s55s\,^3S_1$ two-color two-photon excitation scheme which was driven with copropagating continuous-wave laser beams at wavelengths of 388.975 and 786.817 nm for each step [28]. These laser beams were focused to ~100 μm FWHM waists in the excitation region. The laser used to drive the $1s3p\,^3P_2 \rightarrow 1s55s\,^3S_1$ transition was detuned by $-2\pi \times 90$ MHz from the field-free transition frequency. Since the $|55s\rangle$ state has a quadratic Stark shift and a positive electric dipole polarizability, this allowed a pulsed potential of ~300 mV/cm to be applied to Stark shift the transition into resonance with the laser for a selected period of time. In the experiments described here, this excitation pulse duration was set to 1 μs and resulted in the excitation of ~2-mm-long bunches of excited atoms.

The laser excitation position in the y dimension in the apparatus was adjusted to excite atoms in the beam that propagated close ($\lesssim$ 300 μm) to the surface of the 10 × 10 mm niobium nitride (NbN) superconducting chip. This chip contained an inverted U-shaped coplanar microwave waveguide, capacitively coupled to an L-shaped $\lambda/4$ CPW resonator (see the inset in Fig. 1). The atomic beam was aligned to propagate above the longer (5 mm) straight section of the resonator. The superconducting chip holder, and through this the resonator, was cooled to <4 K. The resonance frequency of the resonator was coarsely adjusted by controlling this temperature T_{res}. To operate at resonator resonance frequencies of $\omega_3 = 2\pi \times 19.556$ GHz or $2\pi \times 19.552$ GHz in the

third-harmonic mode, $T_{\rm res}$ was stabilized to 3.59 or 3.73 K, respectively. At these temperatures, the loaded quality factor in this mode was $Q \simeq 2100$. This corresponds to a FWHM spectral width of $2\pi \times 9.3$ MHz. Under these operating conditions, ω_3 was near resonant with or detuned by $\sim -2\pi \times 4$ MHz from the field-free single-color two-photon transition between the $|55s\rangle$ and $1s56s\,^3S_1 \equiv |56s\rangle$ Rydberg levels that occurs at $\omega_{55s,56s}/2 = 2\pi \times 19.556499$ GHz.

The dc electric fields and microwave-dressing fields were generated above the superconducting chip by applying pulsed offset potentials to the split electrode E3 and driving the microwave antenna, respectively (see Fig. 1). The antenna was located above the gap between the split components of electrode E3 at a distance of 17.5 mm above the NbN chip surface and was orientated in the direction of propagation of the atomic beam. It was designed to operate simultaneously at frequencies around $\omega_{55s,56s}/2 \simeq 2\pi \times 19.556$ GHz and $2\pi \times 9.118$ GHz. A field at the lower frequency was used to null the electric dipole polarizability of the $|55s\rangle \rightarrow |56s\rangle$ transition. During the experiments, microwave pulses of 1-μs duration were applied to the antenna 15 μs after laser photoexcitation of the atoms to the $|55s\rangle$ Rydberg state. These coincided with the injection of similar pulses at an angular frequency $\omega_{\rm res}$ into the CPW resonator from the waveguide on the superconducting chip. At this time, the Rydberg atoms were located above the resonator. The microwave-dressing fields were used in conjunction with the evanescent field of the resonator to probe the atom-resonator coupling, and the tunability and dc electric-field sensitivity of the interface.

At the end of each cycle of the experiment, the populations of the $|55s\rangle$ and $|56s\rangle$ Rydberg states were determined by state-selective pulsed electric-field ionization. This was implemented by applying a slowly rising negative pulsed potential to electrode E4, 25 μs after laser photoexcitation. Since the $|55s\rangle$ Rydberg state ionizes in a higher electric field than the $|56s\rangle$ state, the difference in arrival times of the ionized electrons at a microchannel plate (MCP) detector, located outside the cryogenic region of the apparatus, allowed for efficient and selective determination of the populations of the two states [2].

III. MICROWAVE-DRESSING SCHEMES FOR RYDBERG-STATE CONTROL AND ENGINEERING

The transition between the equal-parity $|55s\rangle$ and $|56s\rangle$ triplet Rydberg states in He can be driven as a single-color two-photon transition at an angular frequency $\omega_{55s,\,56s}/2 = 2\pi \times 19.556499$ GHz, as indicated in Fig. 2(a). These two Rydberg states have comparatively large quantum defects of $\delta_{55s} = 0.2966693$ and $\delta_{56s} = 0.2966688$, respectively [29]. As a result, they are energetically isolated from higher-ℓ Rydberg states, and the difference in their static electric dipole polarizabilities, i.e., their differential static electric dipole polarizability, is $\alpha_{55s,56s} = 0.273\,{\rm GHz/(V/cm)^2}$. This comparatively low differential polarizability leads to an inherently low sensitivity of the microwave transition between these states to weak electric fields [30].

A further consequence of the large quantum defects of these Rydberg states is that the avoided crossings that they undergo with other ℓ-mixed Rydberg states in electric fields

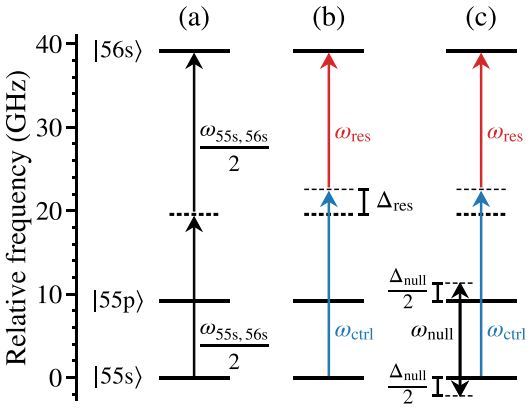

FIG. 2. Energy-level structure and two-photon transitions between the $|55s\rangle$ and $|56s\rangle$ triplet Rydberg states in He. (a) Single-color two-photon transition. (b) Two-color two-photon transition driven by the resonator field $\omega_{\rm res}$ and a control field $\omega_{\rm ctrl}$. (c) Two-color two-photon transition with the addition of a differential polarizability nulling field at a frequency $\omega_{\rm null}$, which is detuned by $\Delta_{\rm null}$ from the single-photon $|55s\rangle \rightarrow |55p\rangle$ transition.

at and beyond the Inglis-Teller limit (the electric field in which Rydberg-Stark states with values of n that differ by $+1$ first cross) are also large. This allows for efficient adiabatic traversal of these crossings during pulsed electric-field ionization and ionization in distinct and narrowly defined ranges of electric fields such that the populations of the two states can be reliably determined in this way [2].

The two-photon $|55s\rangle \rightarrow |56s\rangle$ transition is mediated by the presence of the off-resonant $1s55p\,^3P_J$ ($|55p\rangle$) levels. These levels have fine-structure splittings of $\sim 2\pi \times 1$ MHz [31] but are far off resonance (by $\sim -2\pi \times 10$ GHz) from the single-color two-photon transition frequency. Consequently, the two-photon Rabi frequency, expressed as the product of the single-photon Rabi frequencies for the $|55s\rangle \rightarrow |55p\rangle$ ($\Omega_{55s,\,55p} = F_\mu\, \mu_{55s,\,55p}/\hbar$) and $|55p\rangle \rightarrow |56s\rangle$ ($\Omega_{55p,\,56s} = F_\mu\, \mu_{55p,\,56s}/\hbar$) transitions, is [32]

$$\Omega_{\rm eff} = \frac{\Omega_{55s,\,55p}\,\Omega_{55p,\,56s}}{2\Delta}, \tag{1}$$

where F_μ is the microwave electric-field amplitude and $\mu_{55s,\,55p} = 2457ea_0$ and $\mu_{55p,\,56s} = 1185ea_0$ are the electric dipole transition moments, with e being the electron charge and a_0 being the Bohr radius.

To achieve a high coupling strength between the atoms and the microwave field in the CPW resonator, it is desirable to drive the $|55s\rangle \rightarrow |56s\rangle$ transition as a two-color two-photon transition so that it is necessary to absorb only one photon from the resonator. This can be achieved by dressing the atom with a strong external control field $\omega_{\rm ctrl}$ and arranging that $\omega_{\rm res} = \omega_{55s,\,56s}/2 - \Delta_{\rm res}$ and $\omega_{\rm ctrl} = \omega_{55s,\,56s}/2 + \Delta_{\rm res}$. Here, $\Delta_{\rm res}$ represents the detuning from the single-color two-photon transition frequency, as indicated in Fig. 2(b), and $\omega_{\rm ctl} + \omega_{\rm res} = \omega_{55s,\,56s}$. This approach to exploiting the broad tunability of a strong control field to compensate a detuning of the resonator mode from the single-color two-photon transition frequency establishes the frequency tunability of this quantum interface. Under these conditions, the atom-resonator coupling strength

can then be set by adjusting the strength of the control field. In the dressed-atom picture, the transition between the Rydberg states to which the resonator field is coupled in this scheme is the transition from a microwave-dressed state to a bare state.

To further engineer the $|55s\rangle \rightarrow |56s\rangle$ transition to minimize its sensitivity to dc electric fields, its Stark shift should be minimized. This was achieved here through the application of a second microwave-dressing field at a frequency $\omega_{\rm null}$. This differential polarizability nulling field, or "nulling field," was detuned from the $|55s\rangle \rightarrow |55p\rangle$ transition by $\Delta_{\rm null} = \omega_{\rm null} - \omega_{55s,\,55p}$ [see Fig. 2(c)] to eliminate, or "null," the differential static electric dipole polarizability of the $|55s\rangle$ and $|56s\rangle$ states. The effect of this nulling field can be understood by observing that the polarizability of the $|56s\rangle$ state, $\alpha_{56s} = 2.302\,{\rm GHz/(V/cm)^2}$, is larger than that of the $|55s\rangle$ state, $\alpha_{55s} = 2.029\,{\rm GHz/(V/cm)^2}$. To null the differential polarizability of these two Rydberg states, it is therefore necessary to increase the effective static electric dipole polarizability of the $|55s\rangle$ state or decrease that of the $|56s\rangle$ state. Since the polarizability of the $|55p\rangle$ state, which can be coupled to the $|55s\rangle$ state by a strong single-photon electric dipole transition, is comparatively large [$\alpha_{55p} = 4.834\,{\rm GHz/(V/cm)^2}$], the admixture of some $|55p\rangle$ character into the $|55s\rangle$ state by off-resonant microwave dressing provides a controllable way to enhance the effective polarizability of this state so that it becomes equal to that of the $|56s\rangle$ state. The optimal ratio of $|55s\rangle$ and $|55p\rangle$ character in the resulting dressed state can be set by adjusting the amplitude $F_{\rm null}$ of the nulling field and its detuning $\Delta_{\rm null}$ from the $|55s\rangle \rightarrow |55p\rangle$ transition [26].

The effects of microwave nulling fields and dc electric fields on the $|55s\rangle \rightarrow |56s\rangle$ transition frequency were calculated to determine optimal nulling-field parameters and quantify the effects of these fields. These calculations were performed by considering the Hamiltonian of the Rydberg atom within the electric dipole approximation [26], such that

$$H(t) = H_0 + eF_{\rm dc}z + eF_{\rm null}\cos(\omega_{\rm null}t)z, \tag{2}$$

where H_0 is the field-free Hamiltonian and the dc field $\vec{F}_{\rm dc} = (0, 0, F_{\rm dc})$ and nulling field $\vec{F}_{\rm null} = [0, 0, F_{\rm null}\cos(\omega_{\rm null}t)]$ act in the z dimension. Floquet methods [33] were used to transform this Hamiltonian to obtain a time-independent infinite-dimensional eigenvalue problem with matrix elements

$$\begin{aligned}&\langle n'\ell'm_\ell{}'\,q'_{\rm null}|H_{\rm F}|n\,\ell\,m_\ell\,q_{\rm null}\rangle \\ &\quad = \mathscr{H}^{q_{\rm null}}_{n\ell m_\ell} + \cdots + q_{\rm null}\,\hbar\,\omega_{\rm null}\,\delta_{n,\,n'}\,\delta_{\ell,\,\ell'}\,\delta_{m_\ell,\,m_\ell{}'}\,\delta_{q_{\rm null},\,q'_{\rm null}}.\end{aligned} \tag{3}$$

In this expression, $H_{\rm F}$ is the time-independent Floquet Hamiltonian, which is constructed in the $|n\ell m_\ell\rangle$ basis of atomic orbitals (ℓ and m_ℓ are the orbital angular momentum and azimuthal quantum numbers of the Rydberg electron, respectively). Following this transformation, an infinite set of Fourier sidebands become associated with the nulling field. They are labeled by the integer index $q_{\rm null}$ that ranges from $-\infty$ to $+\infty$. The elements of the matrix $\mathscr{H}^{q_{\rm null}}_{n\ell m_\ell}$ for each value of $q_{\rm null}$ are then

$$\begin{aligned}\mathscr{H}^{q_{\rm null}}_{n\ell m_\ell} &= \langle n'\ell'm_\ell{}'|H_0|n\,\ell\,m_\ell\rangle\,\delta_{q_{\rm null},q'_{\rm null}} + \cdots \\ &+ eF_{\rm dc}\,\langle n'\ell'm_\ell{}'|z|n\,\ell\,m_\ell\rangle\,\delta_{q_{\rm null},q'_{\rm null}} + \cdots \\ &+ \frac{eF_{\rm null}}{2}\langle n'\ell'm_\ell{}'|z|n\,\ell\,m_\ell\rangle\,\delta_{q_{\rm null}\pm1,q'_{\rm null}},\end{aligned} \tag{4}$$

where the first term corresponds to the set of diagonal matrix elements that represent the field-free energies of the Rydberg states, i.e., $\langle n'\ell'm'_\ell|H_0|n\ell m_\ell\rangle = E_{n\ell} = -h\,c\,R_{\rm He}/(n-\delta_{n\ell})^2$. The second and third terms in Eq. (4) represent the interaction of the atom with the dc and time-dependent nulling fields, respectively. The values of these matrix elements were determined by numerical integration [26,34]. For all calculations described here, convergence to within the experimental uncertainties of $\sim 2\pi\times10$ kHz was achieved using a basis of states in which $|q_{\rm null}| \leqslant 1$, $52 \leqslant n \leqslant 58$, with all allowed values of ℓ.

IV. A TUNABLE RYDBERG-ATOM–SUPERCONDUCTING-CIRCUIT INTERFACE

To demonstrate the operation of the tunable interface between the He Rydberg atoms and the superconducting circuit, the coupling of the atoms to the resonator field was probed spectroscopically. Measurements were made with the resonator operated at two temperatures $T_{\rm res}$ and hence resonance frequencies ω_3, and with and without the control field applied.

Reference spectra were recorded with the control field off and the resonator operated at $T_{\rm res} = 3.59$ K, so that $\omega_3 = 2\pi\times19.556\,{\rm GHz} \simeq \omega_{55s\,56s}/2$. They were obtained by scanning the frequency of the pulsed microwave field injected into the resonator from the CPW on the superconducting chip. From these data, presented in Fig. 3(a), the coupling of the atoms to the resonator field through the single-color two-photon $|55s\rangle \rightarrow |56s\rangle$ transition was identified from the population transfer to the $|56s\rangle$ state at a frequency close to $2\pi\times19.556\,{\rm GHz}$ [Fig. 3(a-i)].

The resonance associated with the $|55s\rangle \rightarrow |56s\rangle$ transition in Fig. 3(a-i) is shifted by $-2\pi\times0.7\,{\rm MHz}$ from $\omega_{55s\,56s}/2 = 2\pi\times19.5565\,{\rm GHz}$ (vertical gray dashed line). Since this single-color two-photon transition is driven by the stationary field in the resonator, first-order Doppler shifts do not play a role in these measurements. Consequently, this shift indicates the presence of a residual stray electric field at the position of the atoms above the superconducting chip. A comparison of the measured transition frequency with the calculated dc Stark shift allowed the strength of this field to be determined to be ~85 mV/cm. The cancellation of this residual field was limited in these experiments, compared to earlier work [1–3], because of the presence of the microwave antenna between the two components of the split electrode E3 (this is discussed further in Sec. V).

The power of the microwave field injected from the waveguide into the resonator on the NbN chip when recording the data in Fig. 3(a-i) was $P_{\rm CPW} = P_0 \simeq -11.5$ dBm. To establish conditions under which the contribution of a strong control field could be unambiguously identified, a second similar reference spectrum was recorded with $P_{\rm CPW} = P_0 - 7$ dBm, as shown in Fig. 3(a-ii). The corresponding circulating power

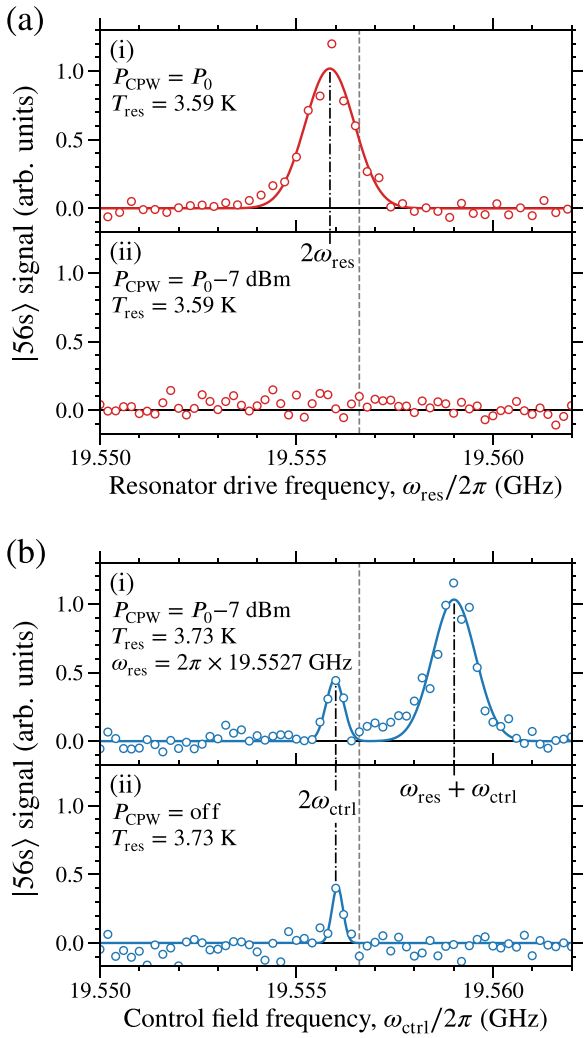

FIG. 3. Microwave spectra of the $|55s\rangle \rightarrow |56s\rangle$ transition at the Rydberg-atom–superconducting-circuit interface. (a) The single-color two-photon transition recorded by scanning the frequency of the microwave field injected into the resonator with $T_{res} = 3.59$ K and $\omega_3 \simeq 2\pi \times 19.556$ GHz, and for (i) $P_{CPW} = P_0$ and (ii) $P_{CPW} = P_0 - 7$ dBm. (b) Spectra recorded for $T_{res} = 3.73$ K and hence $\omega_3 \simeq 2\pi \times 19.552$ GHz by scanning the frequency of the control field (i) with and (ii) without driving the resonator. The gray vertical dashed line spanning both panels represents the field-free single-color two-photon transition frequency (see text for details).

in the resonator was ∼1 mW which does not result in any population transfer at the single-color two-photon transition frequency, indicating that under these resonator driving conditions, an additional field is required to couple the atoms to the resonator.

To exploit the strong control field to demonstrate the frequency tunability of this interface, the resonator temperature was set to $T_{res} = 3.73$ K. This detuned the resonator resonance frequency by $\Delta_{res} = -2\pi \times 3.1$ MHz from the single-color two-photon transition in Fig. 3(a-i). The frequency of the microwave field injected into it was then also detuned by an equal amount and set to $\omega_{res} = 2\pi \times 19.5527$ GHz so that the $|55s\rangle \rightarrow |56s\rangle$ transition could be driven as a two-color two-photon transition. Under these conditions, with $P_{CPW} = P_0 - 7$ dBm, coupling of the atoms to the resonator field can occur only if the atoms are dressed with a strong control field detuned by $\Delta_{res} = +2\pi \times 3.1$ MHz from the measured single-color two-photon transition frequency. The effect of introducing this control field can be seen from the spectrum in Fig. 3(b-i). When these data were recorded, the frequency of the control field emanating from the antenna above the superconducting chip was scanned while the transfer of population to the $|56s\rangle$ state was monitored. In this spectrum, a strong feature is present at a frequency close to $\omega_{ctl} = 2\pi \times 19.5590$ GHz. This represents the two-color two-photon $|55s\rangle \rightarrow |56s\rangle$ transition that occurs upon the simultaneous absorption of one photon from the control field and one photon from the resonator when $\omega_{ctl} + \omega_{res} \simeq \omega_{55s\,56s}$.

From the spectrum in Fig. 3(a-i), the measured value of the total frequency interval between the $|55s\rangle$ and $|56s\rangle$ states in the presence of the residual stray electric field above the NbN chip was found to be $2\pi \times 39.1116$ GHz. However, on the two-color resonance in Fig. 3(b-i), $\omega_{ctl} + \omega_{res} = 2\pi \times (19.5590 + 19.5527) = 2\pi \times 39.1117$ GHz. The difference of $2\pi \times 0.1$ MHz between these angular frequencies is attributed to an ac Stark shift of the transition in the presence of the strong control field.

The spectrum in Fig. 3(b-i) also exhibits a narrow feature at the single-color two-photon transition frequency close to $2\pi \times 19.556$ GHz. This is solely caused by the strong control field, without any contribution from the resonator, as confirmed from the spectrum in Fig. 3(b-ii) in which no microwave field was injected into the resonator. Under these conditions, the strong feature at the two-color two-photon transition frequency is absent, while the narrower resonance at the single-color two-photon transition frequency remains visible. The reduced spectral width of this resonance is a consequence of it being associated with a two-photon process and the possibility for the field emanating from the antenna to address atoms at much larger atom-surface distances than those in the CPW resonator.

V. DIFFERENTIAL POLARIZABILITY NULLING AT A TUNABLE RYDBERG-ATOM–SUPERCONDUCTING-CIRCUIT INTERFACE

A. dc electric-field calibration

To implement differential polarizability nulling at the tunable Rydberg-atom–superconducting-circuit interface and minimize the sensitivity of the $|55s\rangle \rightarrow |56s\rangle$ transition to residual uncanceled dc electric fields, it was first necessary to characterize and calibrate these fields. Throughout this process, the resonator was operated at $T_{res} = 3.59$ K and was used to drive the single-color two-photon transition at frequencies close to $\omega_{55s\,56s}/2$. This allowed the calculated dc Stark shifts of the transition to be used to calibrate the electric fields above the chip without the need to account for ac Stark shifts from another strong microwave-dressing field.

To determine the relationship between the potential V_{app} applied to the split electrode E3 and the dc field strength at the position of the atoms above the CPW resonator, microwave spectra were recorded by scanning the frequency of the pulsed microwave field injected into the resonator. In this way, the

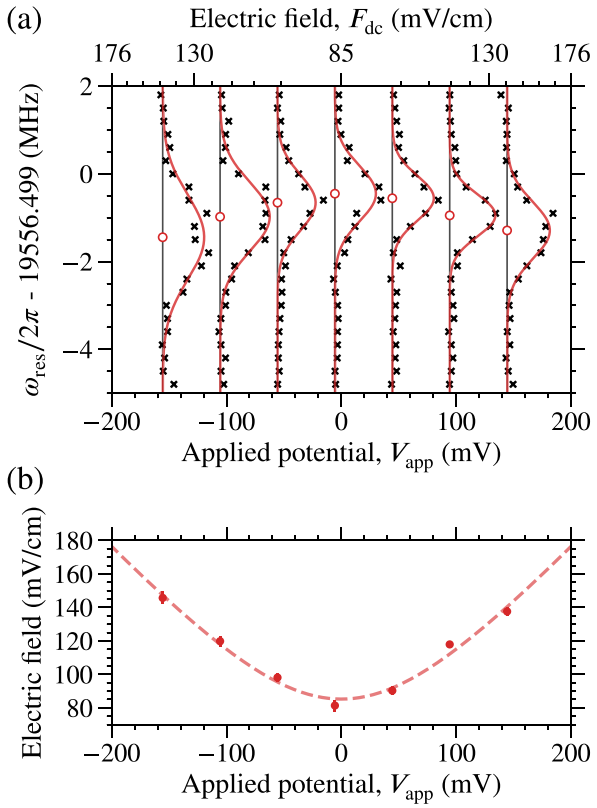

FIG. 4. (a) Stark spectra of the single-color two-photon $|55s\rangle \rightarrow |56s\rangle$ transition driven by the microwave field in the resonator for a range of values of the potential V_{app} applied to E3. (b) Dependence of the dc electric field at the location of the atoms on V_{app} (see text for details).

atoms were used as *in situ* quantum sensors. These spectra, shown in Fig. 4(a), were recorded for values of V_{app} from -160 to $+160$ mV, as indicated on the bottom horizontal axis. To determine the Stark shifts of the transition frequencies, Gaussian functions were fit to these data for each value of V_{app} using least-squares methods. The resulting frequencies are marked by the open red circles beneath each feature and were used to calibrate the strength of the electric field in each case.

The dependence of the measured dc electric field on V_{app} is shown in Fig. 4(b). To obtain an analytic expression for the relationship between $\vec{F}_{dc}$ and V_{app}, it was assumed that the magnitude of $\vec{F}_{dc}$, i.e., $|\vec{F}_{dc}| = F_{dc}$, was dependent on the vector component of the field affected by V_{app} and that this contribution to the resulting field vector contains a constant geometric factor a; therefore,

$$F_{dc} = \sqrt{(aV_{app})^2 + {F_u}^2}, \tag{5}$$

where F_u represents the magnitude of a perpendicular uncanceled electric field that is unaffected by changing V_{app}. By fitting the function in Eq. (5) (dashed curve) to the experimental data in Fig. 4(b), it was found that $F_u = 85$ mV/cm and $a = 0.772$ cm^{-1}. The range of values of F_{dc} generated by applying the offset potentials indicated on the bottom horizontal axis in Fig. 4(a) therefore extended from 85 to 150 mV/cm, as marked on the top horizontal axis. The strength of these dc electric fields, their homogeneity, and the magnitude of the residual uncanceled field of 85 mV/cm at the location of the atoms above the superconducting chip are affected by the presence of the grounded center conductor of the antenna located between the two components of the split electrode E3. Without the antenna, residual uncanceled fields below 30 mV/cm and a more direct relationship between V_{app} and F_{dc} were previously obtained [3].

B. Differential polarizability nulling

To null the polarizability of the $|55s\rangle \rightarrow |56s\rangle$ transition in atoms coupled to the resonator field using the two-color two-photon transition, the resonator temperature was set to $T_{res} = 3.59$ K, and the control and nulling fields were generated above the superconducting chip. These two microwave fields emanated from the same antenna. The frequency of the nulling field ω_{null} was chosen to be off resonant from the strong single-photon $|55s\rangle \rightarrow |55p\rangle$ electric dipole transition. In the absence of external fields, this transition occurs at $\omega_{55s\,55p} = 2\pi \times 9.118568$ GHz.

To use the nulling field to induce an ac Stark shift that balanced the differential dc Stark shift of the $|55s\rangle$ and $|56s\rangle$ states, ω_{null} was positively detuned from $\omega_{55s\,55p}$. In general, if a sufficiently strong nulling field can be generated, the larger the detuning Δ_{null} is, the greater the range of dc fields over which nulling can be achieved for this set of Rydberg states. To null the differential polarizability of the $|55s\rangle$ and $|56s\rangle$ states in dc fields up to $F_{dc} \simeq 150$ mV/cm, a nulling field for which $\Delta_{null} = +2\pi \times 44$ MHz was chosen. The optimal amplitude F_{null} of this field was determined to be 14.8 mV/cm using the methods described in Sec. III [26]. The ac Stark shift of the $|55s\rangle$ state under these optimal nulling conditions and in the presence of the residual uncanceled stray dc field of $F_u = 85$ mV/cm was calculated to be $\Delta^{ac}_{55s} = +2\pi \times 8.5$ MHz. This ac Stark shift was used as the observable with which to optimize the nulling-field strength in the apparatus at the location of the atoms above the superconducting chip.

The effect of differential polarizability nulling on the tunable interface can be seen in the spectra in Fig. 5. They were recorded by driving the resonator on resonance at $\omega_{res} = \omega_3 = 2\pi \times 19.5565$ GHz. This corresponds to the field-free single-color two-photon $|55s\rangle \rightarrow |56s\rangle$ transition frequency. However, in the presence of the nulling field, the ac Stark shift of this transition is more than $-2\pi \times 8$ MHz, and it is therefore detuned from the resonance frequency of the resonator by more than its spectral FWHM. The frequency of the control field ω_{ctl} was scanned to observe the ac-Stark-shifted two-color two-photon transition in the presence of the nulling field. To validate the effectiveness of the differential polarizability nulling, microwave spectra were recorded for a range of applied dc electric fields. These fields were generated by setting the value of V_{app}, and were matched to those for which the calibration procedure described in Sec. V A was implemented. These spectra show that in the presence of the nulling field, the two-photon transition frequency (displayed as the sum of ω_{ctl} and ω_{res}) in Fig. 5 exhibits a combined ac and dc Stark shift of $-2\pi \times 8.5$ MHz and, under the conditions in which the experiments were performed, a mean FWHM spectral

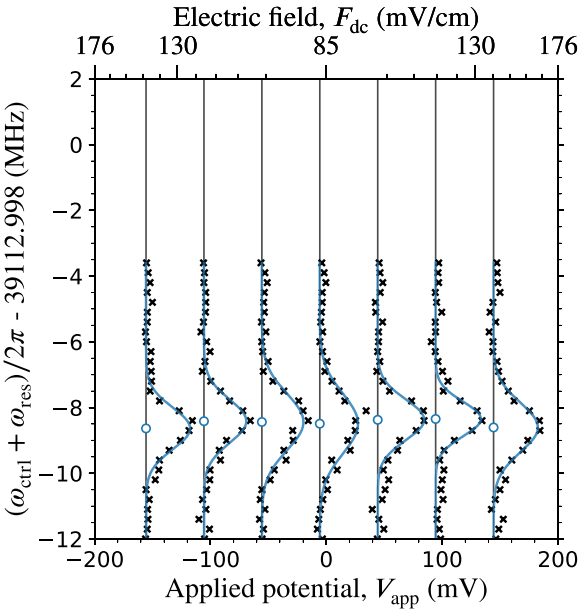

FIG. 5. dc Stark shift of the two-color two-photon $|55s\rangle \rightarrow |56s\rangle$ transition in the presence of the differential polarizability nulling field. These data were recorded by scanning the control-field frequency ω_{ctrl} for a fixed resonator drive frequency of $\omega_{res} = 2\pi \times 19.5565$ GHz.

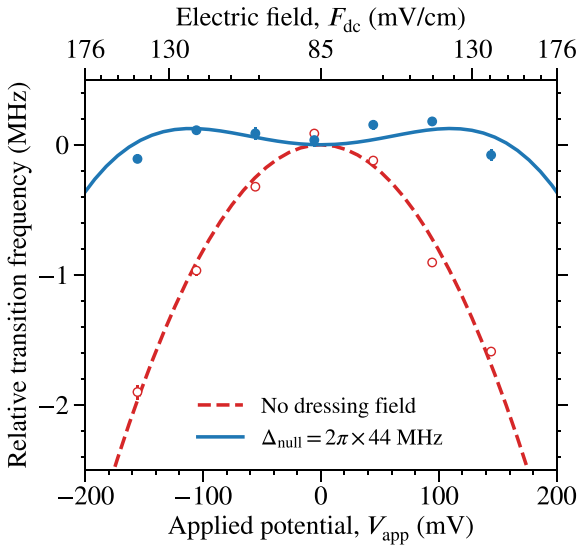

FIG. 6. Differential Stark shift of the $|55s\rangle$ and $|56s\rangle$ states in the absence of microwave-dressing fields (open red points and dashed curve) and with control and nulling fields applied (solid blue points and solid curve). The points represent the measured differential Stark shift of the $|55s\rangle$ and $|56s\rangle$ states obtained from single-color two-photon spectra without the nulling field applied (open red points) and two-color two-photon spectra with the nulling field applied (solid blue points).

width of $2\pi \times 1.6$ MHz. This spectral width is broader than expected from the Fourier transform limit of the 1-μs-duration microwave pulses applied in the measurements. This broadening is attributed to the spatial inhomogeneity of the nulling field above the superconducting chip and the motion of the atoms through this inhomogeneous field. However, for the range of dc electric fields applied, the Stark shift of the polarizability-nulled $|55s\rangle \rightarrow |56s\rangle$ transition remains well within this spectral width for all values of F_{dc} over which measurements were made, i.e., up to $\sim$150 mV/cm.

A quantitative comparison of the measured dc Stark shifts of the two-color $|55s\rangle \rightarrow |56s\rangle$ transition with the results of the Floquet calculations of the energy-level structure of the atom in the presence of the nulling and dc fields is shown in Fig. 6. The solid blue points represent the relative frequencies of the resonances in the two-color two-photon spectra in Fig. 5 These frequencies were determined by fitting Gaussian functions to each spectrum using least-squares methods. For comparison, the measured differential Stark shift of the $|55s\rangle$ and $|56s\rangle$ states, obtained from the single-color two-photon spectra recorded in the absence of these microwave-dressing fields (see Fig. 4), is indicated by the open red points. The dc Stark shifts measured in the absence of the dressing fields are in good quantitative agreement with the calculated Stark shifts obtained from the eigenvalues of the corresponding Hamiltonian matrix (dashed red curve). To calculate the dc Stark shift in the presence of the nulling field, it was necessary to first determine the amplitude F_{null} of this field. It was found from the ac-Stark-shifted $|55s\rangle \rightarrow |56s\rangle$ transition frequency to be $F_{null} = 14.8$ mV/cm. The calculated differential Stark shifts of the $|55s\rangle$ and $|56s\rangle$ states determined from the Floquet calculations in the presence of this nulling field are indicated by the solid blue curve in Fig. 6. The results of these calculations are also in good quantitative agreement with the experimental data. They show that with the nulling field applied, the dc Stark shift of the $|55s\rangle \rightarrow |56s\rangle$ transition, over the range of dc fields offset from the residual stray field by ± 65 mV/cm has been reduced from $2\pi \times 2.1$ MHz to $2\pi \times 125$ kHz. This demonstrates the successful elimination of the differential static electric dipole polarizability of the $|55s\rangle$ and $|56s\rangle$ states.

In these experiments, the range of dc fields over which differential polarizability nulling was achieved was limited by the strength of the nulling field F_{null} that could be generated using the microwave synthesizer that was available. If stronger nulling fields with larger detunings Δ_{null} are employed in the future, this range of dc fields could be further extended [26]. For the $|55s\rangle$ and $|56s\rangle$ states in He, the ultimate limit to this range of $F_{dc} < 250$ mV/cm is set by the proximity of the frequency of the nulling field to the dc-Stark-shifted frequency of the transition between the states that adiabatically evolve into the $|56s\rangle$ and $|56d\rangle$ states in zero field.

VI. CONCLUSIONS

In conclusion, we have coupled microwave-dressed Rydberg atoms to microwave fields in a chip-based superconducting CPW resonator. This was achieved using a two-color two-photon transition between a pair of even-parity Rydberg states. One photon was provided by a strong tunable control field, while the other originated in the resonator. The addition of a polarizability nulling microwave field allowed the static electric dipole polarizability of this tunable Rydberg-atom "qubit" transition to be eliminated.

These results represent a breakthrough in the control and quantum-state engineering of Rydberg atoms at interfaces with superconducting microwave circuits. The broad tunability provided by the control field, and a two-color two-photon transition between Rydberg states of equal parity, opens a path to coupling Rydberg atoms to microwave fields in lower-order, lower-frequency modes of CPW resonators with higher quality factors, and to superconducting qubits with transition frequencies below $2\pi \times 10$ GHz. It also allows for on-demand coupling of the atoms to the resonator field, which lays the foundation for the implementation of quantum memory protocols. The low sensitivity of the polarizability-nulled, tunable Rydberg-atom qubit transition to stray electric fields will, in the future, allow the atoms to be positioned closer to the surface of the superconducting chips without detrimental contributions from these fields. In experiments with more slowly moving atoms and longer atom-resonator interactions times, this will open access to the single-photon strong-coupling regime in this hybrid cavity QED setting. Based on the results reported here, it is anticipated that using the two-photon scheme presented, with a strong control field and weak single-photon absorption from the resonator, vacuum Rabi frequencies on the order of $2\pi \times 1$ MHz can be achieved for atoms located between 30 and 50 μm from the superconducting chip surface. This would be feasible in the current apparatus if improvements were made in positioning the atoms and enhancing the control-field strength. With these improvements, the introduction of electromagnetic fields in the visible and telecom regions that interact with the atoms in the evanescent field above the resonator would allow the implementation of coherent multiwave mixing schemes for optical-to-microwave transduction.

ACKNOWLEDGMENTS

This work was supported the Engineering and Physical Sciences Research Council (EPSRC) through the EPSRC Centre for Doctoral Training in Delivering Quantum Technologies (Grant No. EP/S021582/1). J.A.L.G. is grateful for the support of the Erasmus+ Programme of the European Union.

[1] A. A. Morgan and S. D. Hogan, Coupling Rydberg atoms to microwave fields in a superconducting coplanar waveguide resonator, Phys. Rev. Lett. **124**, 193604 (2020).

[2] D. M. Walker, A. A. Morgan, and S. D. Hogan, Cavity-enhanced Ramsey spectroscopy at a Rydberg-atom–superconducting-circuit interface, Appl. Phys. Lett. **117**, 204001 (2020).

[3] D. M. Walker, L. L. Brown, and S. D. Hogan, Electrometry of a single resonator mode at a Rydberg-atom–superconducting-circuit interface, Phys. Rev. A **105**, 022626 (2022).

[4] M. Kaiser, C. Glaser, L. Y. Ley, J. Grimmel, H. Hattermann, D. Bothner, D. Koelle, R. Kleiner, D. Petrosyan, A. Günther, and J. Fortágh, Cavity-driven Rabi oscillations between Rydberg states of atoms trapped on a superconducting atom chip, Phys. Rev. Res. **4**, 013207 (2022).

[5] A. Blais, A. L. Grimsmo, S. M. Girvin, and A. Wallraff, Circuit quantum electrodynamics, Rev. Mod. Phys. **93**, 025005 (2021).

[6] A. Wallraff, D. I. Schuster, A. Blais, L. Frunzio, R. S. Huang, J. Majer, S. Kumar, S. M. Girvin, and R. J. Schoelkopf, Strong coupling of a single photon to a superconducting qubit using circuit quantum electrodynamics, Nature (London) **431**, 162 (2004).

[7] G. Kurizki, P. Bertet, Y. Kubo, K. Mølmer, D. Petrosyan, P. Rabl, and J. Schmiedmayer, Quantum technologies with hybrid systems, Proc. Natl. Acad. Sci. USA **112**, 3866 (2015).

[8] P. Rabl, D. DeMille, J. M. Doyle, M. D. Lukin, R. J. Schoelkopf, and P. Zoller, Hybrid quantum processors: Molecular ensembles as quantum memory for solid state circuits, Phys. Rev. Lett. **97**, 033003 (2006).

[9] K. Tordrup, A. Negretti, and K. Mølmer, Holographic quantum computing, Phys. Rev. Lett. **101**, 040501 (2008).

[10] M. Hafezi, Z. Kim, S. L. Rolston, L. A. Orozco, B. L. Lev, and J. M. Taylor, Atomic interface between microwave and optical photons, Phys. Rev. A **85**, 020302(R) (2012).

[11] D. Petrosyan, K. Mølmer, J. Fortágh, and M. Saffman, Microwave to optical conversion with atoms on a superconducting chip, New J. Phys. **21**, 073033 (2019).

[12] M. Kiffner, A. Feizpour, K. T. Kaczmarek, D. Jaksch, and J. Nunn, Two-way interconversion of millimeter-wave and optical fields in Rydberg gases, New J. Phys. **18**, 093030 (2016).

[13] T. Vogt, C. Gross, J. Han, S. B. Pal, M. Lam, M. Kiffner, and W. Li, Efficient microwave-to-optical conversion using Rydberg atoms, Phys. Rev. A **99**, 023832 (2019).

[14] A. S. Sørensen, C. H. van der Wal, L. I. Childress, and M. D. Lukin, Capacitive coupling of atomic systems to mesoscopic conductors, Phys. Rev. Lett. **92**, 063601 (2004).

[15] L. Sárkány, J. Fortágh, and D. Petrosyan, Long-range quantum gate via Rydberg states of atoms in a thermal microwave cavity, Phys. Rev. A **92**, 030303(R) (2015).

[16] B. Vermersch, P.-O. Guimond, H. Pichler, and P. Zoller, Quantum state transfer via noisy photonic and phononic waveguides, Phys. Rev. Lett. **118**, 133601 (2017).

[17] L. Sárkány, J. Fortágh, and D. Petrosyan, Faithful state transfer between two-level systems via an actively cooled finite-temperature cavity, Phys. Rev. A **97**, 032341 (2018).

[18] T. Thiele, J. Deiglmayr, M. Stammeier, J.-A. Agner, H. Schmutz, F. Merkt, and A. Wallraff, Imaging electric fields in the vicinity of cryogenic surfaces using Rydberg atoms, Phys. Rev. A **92**, 063425 (2015).

[19] H. Hattermann, M. Mack, F. Karlewski, F. Jessen, D. Cano, and J. Fortágh, Detrimental adsorbate fields in experiments with cold Rydberg gases near surfaces, Phys. Rev. A **86**, 022511 (2012).

[20] A. A. Morgan, V. Zhelyazkova, and S. D. Hogan, Preparation of circular Rydberg states in helium with $n \geqslant 70$ using a modified version of the crossed-fields method, Phys. Rev. A **98**, 043416 (2018).

[21] P. Hyafil, J. Mozley, A. Perrin, J. Tailleur, G. Nogues, M. Brune, J. M. Raimond, and S. Haroche, Coherence-preserving trap architecture for long-term control of giant Ryberg atoms, Phys. Rev. Lett. **93**, 103001 (2004).

[22] L. A. Jones, J. D. Carter, and J. D. D. Martin, Rydberg atoms with a reduced sensitivity to dc and low-frequency electric fields, Phys. Rev. A **87**, 023423 (2013).

[23] Y. Ni, P. Xu, and J. D. D. Martin, Reduction of the dc-electric-field sensitivity of circular Rydberg states using nonresonant dressing fields, Phys. Rev. A **92**, 063418 (2015).

[24] D. W. Booth, J. Isaacs, and M. Saffman, Reducing the sensitivity of Rydberg atoms to dc electric fields using two-frequency ac field dressing, Phys. Rev. A **97**, 012515 (2018).

[25] J. C. Bohorquez, R. Chinnarasu, J. Isaacs, D. Booth, M. Beck, R. McDermott, and M. Saffman, Reducing Rydberg-state dc polarizability by microwave dressing, Phys. Rev. A **108**, 022805 (2023).

[26] L. L. Brown and S. D. Hogan, Tunable Rydberg–Rydberg transitions in helium with reduced sensitivity to dc electric fields by two-colour microwave dressing, J. Phys. B **56**, 205001 (2023).

[27] T. Halfmann, J. Koensgen, and K. Bergmann, A source for a high-intensity pulsed beam of metastable helium atoms, Meas. Sci. Technol. **11**, 1510 (2000).

[28] S. D. Hogan, Y. Houston, and B. Wei, Laser photoexcitation of Rydberg states in helium with $n>$ 400, J. Phys. B **51**, 145002 (2018).

[29] G. W. Drake, High precision theory of atomic helium, Phys. Scr. **T83**, 83 (1999).

[30] M. Peper, J. Deiglmayr, F. Merkt, C. Sanna, and H. B. van Linden van den Heuvell, Magic Rydberg-Rydberg transitions in electric fields, Phys. Rev. A **100**, 032512 (2019).

[31] A. Deller and S. D. Hogan, Microwave spectroscopy of the $1snp\,^3P_J$ fine structure of high Rydberg states in ^{4}He, Phys. Rev. A **97**, 012505 (2018).

[32] T. R. Gentile, B. J. Hughey, D. Kleppner, and T. W. Ducas, Experimental study of one- and two-photon Rabi oscillations, Phys. Rev. A **40**, 5103 (1989).

[33] J. H. Shirley, Solution of the Schrödinger equation with a Hamiltonian periodic in time, Phys. Rev. **138**, B979 (1965).

[34] M. L. Zimmerman, M. G. Littman, M. M. Kash, and D. Kleppner, Stark structure of the Rydberg states of alkali-metal atoms, Phys. Rev. A **20**, 2251 (1979).